



# Adaptive Neural Network-Based Dynamic Surface Control for a 3-DoF Helicopter

M. Abolfazl Mokhtari<sup>1</sup> 

Received: 6 December 2022 / Revised: 11 January 2024 / Accepted: 13 January 2024 / Published online: 4 March 2024  
© Brazilian Society for Automatics–SBA 2024

## Abstract

This paper presents a new robust control structure to control a 3-degree-of-freedom (3-DoF) helicopter in the presence of uncertainties, disturbance and actuators saturation. The 3-DoF helicopter is an underactuated system where only two DoFs can be fully controlled, so elevation and pitching motions are considered in this paper. Robust control methods conventionally generate control signals with high amplitude to suppress model uncertainties. Nonetheless, the practical actuators might not be able to supply such control efforts, causing actuator saturation. The actuator saturation phenomenon highly affects the motion control performance of the system and even can cause instability. To address this issue in this paper, firstly a smooth prevention function is utilized as an approximation of the practical actuator saturation, limiting the input torque/force in a prescribed range. However, to avoid violating the stability of the system by a prevention function, it should be considered in the dynamic model of the system, leading to a non-affine structure. Hence, the problem of controlling a non-affine system is addressed by proposing a new third-order dynamic model, as well as a robust control scheme. In this approach, a backstepping control is utilized, equipped with an adaptive radial basis function neural network to estimate and compensate for the adverse terms. Finally, the effectiveness of the proposed scheme is evaluated through a detailed simulation study on a 3-DoF helicopter.

**Keywords** Adaptive neural network · Robust control · 3-DoF helicopter · Dynamic surface control · Backstepping control · Lyapunov analysis

## 1 Introduction

Autonomous unmanned aerial vehicles (AUAV) have been the focus of research due to their high flight flexibility. These vehicles have been used in various applications such as rescue missions (Bravo et al., 2019), mapping for 3D reconstruction purposes (Saska et al., 2017), civil applications (Finn & Wright, 2012) and use in wireless network (Jawhar et al., 2016), as well as traffic monitoring (Kanistras et al., 2013). In recent years, control researchers have paid more attention to the 3-degree-of-freedom (DoF) laboratory helicopter, which is considered a type of the AUAV (Castañeda et al., 2016). Despite the simple mechanical structure of the 3-DoF helicopter, it is a very complex system from the control point of view due to the nonlinearity, model uncertainties and external disturbances (Zhu & Li, 2021). The control problem of the

3-DoF helicopter has been studied through different control approaches.

In recent decades, various types of controllers are proposed and applied to a 3-DoF helicopter.

In Meza-Sánchez et al. (2015), a sliding mode controller is designed along with a velocity sliding mode observer. It should be noted that the sliding mode-based methods suffer from the chattering phenomenon. In another study, a decentralized consensus control is developed for multiple helicopters with a disturbance estimator in the presence of uncertainties (Li et al., 2015). An uncertainty estimator is designed to observe the unknown dynamics in Zhu et al. (2015). In Guzey et al. (2019), an LQR controller is combined with a sliding surface to deal with the external disturbance and model uncertainty. Note that the utilized LQR method depends on the linear dynamic model around the equilibrium point, so it will be highly affected by the model uncertainty, originating from the model linearization. In addition, the control efforts have large values and the chattering phenomenon happens as a result of the dominant effect of the model uncertainty, which is mainly due to the model linearization. In

✉ M. Abolfazl Mokhtari  
s.abolfazlmokhtari@aut.ac.ir

<sup>1</sup> Engineering and Flight Department, Imam Ali University, Imam Khomeini Street, Tehran, Tehran 1317893471, Iran

Chaoui and Yadav (2020), an adaptive control algorithm is designed to stabilize a 3-DoF helicopter subjected to structured and unstructured model uncertainty. In this study, the parameters of the system are estimated through online learning of the inverse dynamic model. In another study (Li et al., 2018), an output backstepping control along with a state observer is developed to estimate the velocity state to be used in the control scheme. It is claimed that the control approach is robust; however, the effects of the model uncertainties and the external disturbance are ignored. In Castañeda et al. (2016), a continuous differentiator along with an adaptive super twisting scheme is proposed for a 3-DoF helicopter in the presence of the model uncertainties. In this method, a continuous differentiator is used to estimate the state of the system. In this case, replacing the inverse dynamic with the adaptation law results in a higher control effort which in turn requires high-power actuators. Although there has been much research focused on the control of the 3-DoF Helicopter, there are some practical issues like actuator saturation which are less noticed in nonlinear control design. The actuator saturation is a practical problem that arises as a constraint on the control effort. This issue may diminish the performance and effectiveness of the control systems and in some cases even may lead to instability of the closed-loop systems (Lin, 1995).

The actuators saturation problem has been addressed for several nonlinear systems such as cable robots (Ameri et al. 2021a, 2021c) and surface vessels (Zheng et al., 2017). Generally, there are two well-known methods for tackling actuator saturation: observer-based approaches (Fazeli et al., 2022) and dynamic surface control schemes (Ameri et al., 2021b, 2023). The observer-based control design is addressed in several researches to deal with the actuators saturation (Lan et al., 2017a, 2017b; Chen et al., 2015). One of the limitations of the observer-based method for compensating for the actuator saturation is a practical limitation in terms of the real-time computation requirements. It is mainly due to the fact that the response of the observers in practice should be faster than the actual dynamic (Bu et al., 2015). This requirement obliges the designer to have a higher sampling rate for the control loop, which is costly both in terms of the instrumentation and the real-time computation. As mentioned earlier, the other method to deal with actuator saturation is the dynamic surface control approach. In Mousavi and Khayatian (2011, 2016), a backstepping-based dynamic surface control scheme is introduced, which is developed for a class of uncertain saturated systems. In Ponce et al. (2018), a robust controller based on  $H_\infty$  synthesis is designed to control a 3-DoF helicopter in the presence of dead-zone phenomenon in the actuators. This is done through the online linearization of the actual nonlinear dynamic of the system. One of the shortcomings of this method is the computation time for online linearization, leading to delays in

practice. In Fischer et al. (2013), a continuous robust integral of the sign of the error control law is proposed for a class of second-order nonlinear systems with a hyperbolic tangent-based saturation approximation. In another study (Liu, 2017), an adaptive backstepping control scheme with a new saturation approximation function is developed for a class of uncertain nonlinear systems. Apart from the above, several researches have been conducted on the theory part of controlling uncertain systems under input saturation (Wen et al., 2011). However, they are limited to the specific classes of uncertain systems, and there is no general method that can include different kinds of uncertainties as a unified approach to be applicable to the 3-DoF helicopter. Moreover, the theoretical outcomes of such researches cannot be directly applied to the AUAV systems. It is mainly due to their specific definition of the considered class of nonlinear dynamic model. On the other hand, the purely backstepping control is not robust under the model uncertainties and external disturbance. Hence, it has to be used along with another auxiliary controller to guarantee robustness under the model uncertainties and external disturbance.

In this paper, a robust constrained control approach is developed for the 3-DoF helicopter system subjected to the actuator saturation problem, model uncertainties and external disturbance. In this approach, a dynamic surface backstepping control equipped with an adaptive radial basis function (RBF) neural network (NN) is utilized to be robust under the dynamic model uncertainties and external disturbances. In addition, a prevention function is used as a smooth approximation model of the actuator saturation to avoid the undesirable effects of the non-smooth saturation function. Moreover, a Nussbaum-type function is utilized to deal with the complex problem of the inverse calculation of the first derivative of the prevention function. Besides, the weights of the utilized RBF NN are designed as an adaptive law, ensuring the network does not violate the system stability. The closed-loop stability of the overall system is analyzed through Lyapunov's second method. Finally, a simulation study is performed in detail to evaluate the performance of the proposed approach.

The remainder of the paper is organized as follows. The preliminaries are introduced in Sect. 2. The problem statement is given in Sect. 3. The control design is developed in Sect. 4. The stability analysis is discussed in Sect. 5. In Sect. 6, the simulation study is performed on a 3-DoF helicopter, and in Sect. 7, the paper is concluded.

## 2 RBF Neural Network

In this section, an overview of RBF NN is presented to be used in the control approach. Radial basis function neural network is a compact network with three layers of input,

hidden and output. It is designed to estimate unknown continuous nonlinear functions with the least error. In this type of network, the hidden layer neurons are utilized by an RBF function. The Gaussian function of the desired RBF network is defined as follows:

$$g(x) = \exp\left(-\frac{x^2}{2\sigma^2}\right), \tag{1}$$

where  $\sigma$  is the standard deviation. To have a desirable estimation performance of the NN, its adjustable weights must be set correctly in which the estimation error converges to a small vicinity of the origin. Suppose that  $x$ ,  $q$  and  $W$  are the network input, the number of hidden layer nodes and the network weights, respectively. The RBF network algorithm is defined as follows (Park & Sandberg, 1991):

$$\begin{cases} h_j = g((x - c_j^2)/b_j^2), \\ f(x) = W^T h(x) + \varepsilon, \end{cases} \tag{2}$$

where  $h = [h_1, \dots, h_q]^T$  is a vector of the Gaussian function  $h_j$  of all of the hidden layers  $q$ ,  $c_j$  is the  $j$ th neuron's center point, and  $b_j$  is the width of the Gaussian basis function. The RBF network is used to estimate the function  $f(\cdot)$ , whose propagation error is  $\varepsilon \leq \varepsilon_N$  in which  $\varepsilon_N$  is a bounded upper bound. Moreover, the estimation of  $f(\cdot)$ , which is the network output, is designed as follows:

$$\hat{f}(x) = \hat{W}^T h(x), \tag{3}$$

where  $\hat{W}$  is the adapted weight such that the NN estimation error tends to a small vicinity of the origin. Moreover, the adaptation law of the network weights should be designed to ensure closed-loop system stability. It is to be noted that the adaptive weights are states of the closed-loop system. Therefore, they should also be incorporated in the Lyapunov candidate function through the stability analysis procedure to ensure the overall system stability.

### 3 Problem Statement

The general dynamic of a 3-DoF helicopter includes three motions of elevation, travel and pitch, which are specified in the schematic plan of a 3-DoF represented in Fig. 1. As this type of helicopter possesses only two actuators, the control scheme can just force two system states to follow a desired path and the remained state follows a trajectory that depends on the motions of the other states. In this paper, the dynamics of elevation and pitch motions are considered for motion control. Hence, the dynamic equations of a 3-DoF Helicopter

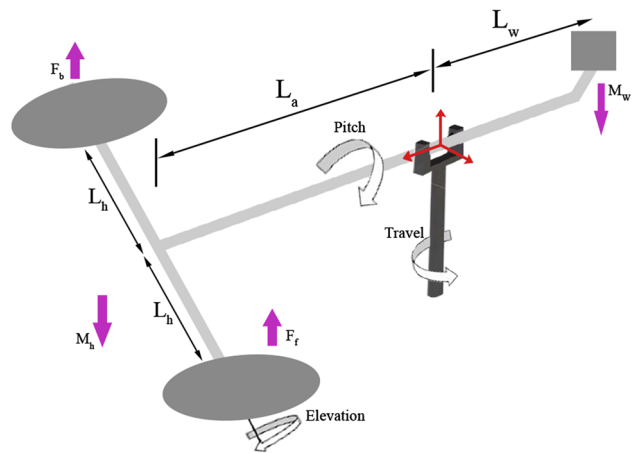


Fig. 1 Schematic plan of a 3-DoF helicopter

are represented according to Lan et al. (2017b), as follows:

$$\begin{cases} \ddot{\alpha} = \frac{k_f L_a}{J_\alpha} (u_1 + u_2) \cos(\gamma) - \frac{(M_h g L_a)}{J_\alpha} \sin(\alpha) + \zeta_\alpha, \\ \ddot{\gamma} = \frac{k_f L_h}{J_\gamma} (u_1 - u_2) + \zeta_\gamma, \end{cases} \tag{4}$$

where  $\alpha$  and  $\gamma$  are the elevation and pitch angles, respectively. Furthermore,  $k_f$  is the propeller force-thrust constant,  $g$  is the gravity acceleration,  $L_a$  is the distance between the travel axis and the helicopter body,  $L_h$  is the distance between the pitch axis and each motor,  $M_h$  is the mass of the helicopter, and  $J_\alpha$  and  $J_\gamma$  are the moments of inertia of the elevation and pitch axes, respectively. Moreover,  $\zeta_\alpha$ ,  $\zeta_\gamma$ ,  $u_1$  and  $u_2$  are the external disturbances and unmodeled dynamics of the elevation and pitch channels and the control input of the front and back motors, respectively.

In order to simplify the dynamic equations, without loss of generality, the augmented motion, control input and disturbance are defined as  $\mathbf{x} = [\alpha \ \gamma]^T$ ,  $\mathbf{u} = [u_1 \ u_2]^T$  and  $\boldsymbol{\zeta}_{aug} = [\zeta_\alpha \ \zeta_\gamma]^T$ , respectively. It is worth noting that the actuator saturation constraint on the control input is considered in this work as a nonlinear prevention function  $\mathbf{u}_{sat} = \boldsymbol{\Omega}(\mathbf{u})$ , which affects the actuators input  $\mathbf{u}$ . Thus, (4) is rewritten as:

$$\ddot{\mathbf{x}} = \boldsymbol{\phi}(\mathbf{x}) + \boldsymbol{\xi}(\mathbf{x})\mathbf{u}_{sat} + \boldsymbol{\zeta}_{aug}. \tag{5}$$

In (5), the nonlinear vector  $\boldsymbol{\phi}(\mathbf{x})$  and nonlinear matrix  $\boldsymbol{\xi}(\mathbf{x})$  are defined as follows:

$$\begin{aligned} \boldsymbol{\phi}(\mathbf{x}) &= \begin{bmatrix} -\frac{(M_h g L_a)}{J_\alpha} \sin(x_1) \\ 0 \end{bmatrix}, \\ \boldsymbol{\xi}(\mathbf{x}) &= \begin{bmatrix} b_1 \cos(x_2) & b_1 \cos(x_2) \\ b_2 & -b_2 \end{bmatrix}, \end{aligned} \tag{6}$$

where  $b_1 = \frac{k_f L_a}{J_\alpha}$  and  $b_2 = \frac{k_f L_h}{J_\gamma}$ .

**Remark 1** The nonlinear prevention function in this work is selected as a differentiable hyperbolic tangent function, as below:

$$\Omega(u) = u_m \tanh\left(\frac{u}{u_m}\right), \tag{7}$$

where  $u_m$  is the bound of the saturation constraint.

**Remark 2** As the actuator saturation is treated in this research by posing a prevention function on the designed control input  $u$ , the resultant generated  $u$  is passed through the prevention function before being fed to the actuator.

**Assumption 1** The control input  $u$ , in this paper, is continuous and differentiable with the first derivative being

$$\dot{u} = \psi. \tag{8}$$

Therefore, designing  $\psi$  as the new controller for the system,  $\dot{u}$  is determined. Thereafter,  $u$  is derived by integrating from  $\dot{u}$ .

### 4 Control Design

In the previous section, (5) represents a non-affine dynamic equation with respect to the control input  $u$ , meaning non-linear dependency on the control input. It is worth noting that the traditional control methods have been developed for affine system and there is no general method to generalize them to the non-affine systems. To address this problem in this section, the dynamic is changed to an affine third-order dynamic equation of motion. Consider the saturated control input  $u_{sat}$  as a new system state, we have:

$$\chi = u_{sat}. \tag{9}$$

Taking the first derivative of (9) and using (8) yield:

$$\dot{\chi} = \frac{\partial \Omega}{\partial u} \psi. \tag{10}$$

To describe the entire dynamic of the third-order system in state space form, new states can be defined as:

$$\begin{cases} z_1 = x, \\ z_2 = \dot{x}, \\ z_3 = \chi. \end{cases} \tag{11}$$

Differentiating (11) and using (10) and (5), the third-order dynamic equation of the 3-DoF helicopter in the presence of

actuator saturation is described in the state space form as:

$$\begin{cases} \dot{z}_1 = z_2, \\ \dot{z}_2 = \phi(z_1) + \xi(z_1)z_3 + \zeta_{aug}, \\ \dot{z}_3 = \frac{\partial \Omega}{\partial u} \psi. \end{cases} \tag{12}$$

Note that the above dynamic system is affine with respect to the control input  $\psi$ . Besides, the model uncertainties are supposed to be as follows:

$$\begin{cases} \phi(z_1) = \hat{\phi}(z_1) + \Delta\phi, \\ \xi(z_1) = \hat{\xi}(z_1) + \Delta\xi, \end{cases} \tag{13}$$

where  $\hat{\ast}$  and  $\Delta\ast$  represent the nominal values and the uncertainty terms, respectively. Substituting (13) into (12) results in:

$$\begin{cases} \dot{z}_1 = z_2, \\ \dot{z}_2 = \hat{\phi}(z_1) + \hat{\xi}(z_1)z_3 + \zeta, \\ \dot{z}_3 = \frac{\partial \Omega}{\partial u} \psi, \end{cases} \tag{14}$$

where  $\zeta = \zeta_{aug} + \Delta\phi + \Delta\xi z_3$  includes all the disturbances and uncertainties in the system. As the control purpose is trajectory tracking, the following tracking errors are defined:

$$\mu_1 = z_1 - x_d, \tag{15}$$

$$\mu_2 = z_2 - \sigma_1, \tag{16}$$

$$\mu_3 = z_3 - \sigma_2, \tag{17}$$

in which  $x_d$ ,  $\sigma_1$  and  $\sigma_2$  are the desired trajectories to be followed by the angular velocities of the helicopter, the designable desired trajectories for  $z_2$  and  $z_3$  which works as a virtual controller in the first and second steps in the backstepping control scheme, respectively.

According to the backstepping control nature, the following three steps are allocated to propose the control scheme for each subsystem of the third-order dynamic system of the errors (15), (16), (17).

#### 4.1 First Step

Taking the first derivative of (15) and using (14), one can write:

$$\dot{\mu}_1 = z_2 - \dot{x}_d. \tag{18}$$

From (16), we have:

$$\dot{\mu}_1 = \mu_2 + \sigma_1 - \dot{x}_d, \tag{19}$$

where  $\sigma_1$  acts as a virtual controller for this dynamic subsystem. The virtual control law  $\sigma_1$  is designed to stabilize this

dynamic equation, as follows:

$$\sigma_1 = \dot{x}_d - \lambda_1 \mu_1, \quad (20)$$

where  $\lambda_1$  is a diagonal positive definite matrix.

The Lyapunov function  $V_1 = \frac{1}{2}(\mu_1^T \mu_1)$  is selected to evaluate the stability of the first subsystem. Taking its first derivative and substituting (19), we have:

$$\dot{V}_1 = \mu_1^T \dot{\mu}_1 = \mu_1^T (\mu_2 + \sigma_1 - \dot{x}_d). \quad (21)$$

Recalling the designed virtual control (20) and simplifying yield:

$$\dot{V}_1 = -\mu_1^T \lambda_1 \mu_1 + \mu_1^T \mu_2. \quad (22)$$

## 4.2 Second Step

The dynamic equation of the second subsystem can be provided by taking the derivative of (16), which results in:

$$\dot{\mu}_2 = \hat{\phi}(z_1) + \hat{\xi}(z_1)(\mu_3 + \sigma_2) + \zeta - \dot{\sigma}_1. \quad (23)$$

It is to be noted that  $\zeta$  is estimated in this paper using RBF NN, so it is considered as  $\zeta = \omega^T \theta$  where  $\omega$  represents the actual network weights and  $\theta$  stands for the basis function vector. In (23),  $\sigma_2$  plays the virtual controller role for (23), so it should be designed to stabilize the dynamic subsystem (23). Hence, this virtual controller is proposed as:

$$\sigma_2 = \hat{\xi}^{-1}(z_1)(-\hat{\phi}(z_1) - \hat{\omega}^T \theta(z_1) + \dot{\sigma}_1 - \lambda_2 \mu_2 - \mu_1), \quad (24)$$

where  $\lambda_2$  is a diagonal positive definite matrix. The stability of the second subsystem with the virtual controller, proposed in (24), is analyzed via the following candidate Lyapunov function:

$$V_2 = \frac{1}{2}(\mu_2^T \mu_2 + tr(\tilde{\omega}^T \Lambda^{-1} \tilde{\omega})). \quad (25)$$

In this function,  $\tilde{\omega} = \hat{\omega} - \omega$  is the adaptation errors of the NN weights,  $\hat{\omega}$  is the estimated value for the NN weights using an adaption law and  $\Lambda$  is an invertible diagonal positive definite matrix. Taking the first derivative of the Lyapunov function with respect to time and substituting (23) result in:

$$\begin{aligned} \dot{V}_2 &= \mu_2^T \dot{\mu}_2 + tr(\tilde{\omega}^T \Lambda^{-1} \dot{\tilde{\omega}}) \\ &= \mu_2^T (\hat{\phi}(z_1) + \hat{\xi}(z_1)(\mu_3 + \sigma_2) \\ &\quad + \zeta - \dot{\sigma}_1) + tr(\tilde{\omega}^T \Lambda^{-1} \dot{\tilde{\omega}}). \end{aligned} \quad (26)$$

Substituting (24) into (26), sorting and simplifying yield:

$$\dot{V}_2 = \mu_2^T \hat{\xi}(z_1) \mu_3 - \mu_2^T \lambda_2 \mu_2 - \mu_2^T \mu_1$$

$$+ tr(\tilde{\omega}^T [\Lambda^{-1} \dot{\tilde{\omega}} - \theta(z_1) \mu_2^T]). \quad (27)$$

As mentioned earlier, an RBF NN is utilized to achieve robust performance in the presence of dynamic uncertainties and external disturbances. Hence, there is still a requirement to design an adaptation law for the NN weights to update them online. Therefore, the adaptation law is proposed as follows:

$$\dot{\hat{\omega}} = \Lambda \theta \mu_2^T. \quad (28)$$

Substituting (28) into (27) yields:

$$\dot{V}_2 = \mu_2^T \hat{\xi}(z_1) \mu_3 - \mu_2^T \lambda_2 \mu_2 - \mu_2^T \mu_1. \quad (29)$$

## 4.3 Third Step

The dynamic equation of  $\mu_3$  is created by taking the first derivative of (17) and using (14), as:

$$\dot{\mu}_3 = \frac{\partial \Omega}{\partial u} \psi - \dot{\sigma}_2. \quad (30)$$

Hence, (30) is controlled via proposing an adaptive NN backstepping control scheme, as follows:

$$\psi = F(\rho) \bar{\psi}, \quad (31)$$

$$\bar{\psi} = \dot{\sigma}_2 - \hat{\xi}^T(z_1) \mu_2 - \lambda_3 \mu_3, \quad (32)$$

where  $\lambda_3$  is a diagonal positive definite matrix, and  $F_i(\rho_i)$  is a Nussbaum-type function which is defined as:

$$\begin{cases} F_i(\rho_i) = \rho_i^2 \cos(\rho_i), \\ \dot{\rho}_i = \vartheta \psi_i \mu_{3i}, \end{cases} \quad (33)$$

in which  $\vartheta$  is a positive constant parameter. The following definition is given for the Nussbaum function.

**Definition 1** Wen et al. (2011): If the following equations held for a function  $F(n)$ , thus it is a Nussbaum function.

$$\begin{cases} \lim_{k \rightarrow \pm\infty} \sup \frac{1}{k} \int_0^k F(n) dn = +\infty, \\ \lim_{k \rightarrow \pm\infty} \inf \frac{1}{k} \int_0^k F(n) dn = -\infty. \end{cases} \quad (34)$$

The stability of this subsection is also assessed via the Lyapunov function selected as  $V_3 = \mu_3^T \mu_3$ . Taking the first derivative of this Lyapunov function with respect to time and substituting (30), one may write:

$$\dot{V}_3 = \mu_3^T \dot{\mu}_3 = \mu_3^T \left( \frac{\partial \Omega}{\partial u} \psi - \dot{\sigma}_2 \right). \quad (35)$$



Substituting (31) into (35) yields:

$$\dot{V}_3 = \mu_3^T \left( \frac{\partial \Omega}{\partial u} F(\rho) - I_2 \right) \bar{\psi} + \mu_3^T (\bar{\psi} - \dot{\sigma}_2). \tag{36}$$

Using (33) and (32), we have:

$$\begin{aligned} \dot{V}_3 = & -\mu_3^T \hat{\xi}^T(z_1) \mu_2 - \mu_3^T \lambda_3 \mu_3 \\ & + \frac{1}{\vartheta} \sum_{i=1}^2 \left( \frac{\partial \Omega}{\partial u_i} F_i(\rho_i) - 1 \right) \dot{\rho}_i. \end{aligned} \tag{37}$$

The present section is allocated to the stability of the sub-systems, while the next section presents the stability analysis of the entire system using the results achieved in the present section.

### 5 Stability Analysis

To analyze the stability of the overall third-order dynamic equations of the system, Theorem 1 is illustrated after Lemma 1 which is used in the proof of the theorem.

**Lemma 1** Wen et al. (2011): *Let  $F(\rho_i)$  be a Nussbaum function and  $V(\cdot)$  and  $\rho$  be smooth functions defined on  $[0, t_f]$  with  $V(t) \geq 0$  and  $\forall t \in [0, t_f]$ , and assume that the following inequality is held:*

$$V(t) \leq V(0)e^{-ct} + \frac{e^{-ct}}{\vartheta} \int_0^t \sum_{i=1}^2 \left( \frac{\partial \Omega}{\partial u_i} F_i - 1 \right) \dot{\rho}_i e^{c\tau} d\tau, \tag{38}$$

in which  $c > 0$ ,  $\frac{\partial \Omega}{\partial u_i} > 0$  and  $\vartheta > 0$ . Thus,  $V(\cdot)$ ,  $\rho_i$  and  $\sum_{i=1}^2 \left( \frac{\partial \Omega}{\partial u_i} F_i - 1 \right) \dot{\rho}_i e^{c\tau} d\tau$  are bounded on  $[0, t_f]$ .

**Theorem 1** *Consider the closed-loop system of a 3-DoF helicopter with the dynamic equations (4), input prevention function (7), dynamical control law (8) and the proposed control law (31) along with the adaptation law of the NN weights (28) and the Nussbaum function (33) is stable and all the signals of the system are proved to be bounded.*

**Proof** The following Lyapunov function, including the candidate functions of the three subsystems, is selected as follows:

$$V = V_1 + V_2 + V_3. \tag{39}$$

Taking the first derivative of (39) with respect to time yields:

$$\dot{V} = \dot{V}_1 + \dot{V}_2 + \dot{V}_3. \tag{40}$$

Substituting (22), (29) and (37) into (40), simplifying and sorting result in:

$$\begin{aligned} \dot{V} = & -\mu_1^T \lambda_1 \mu_1 - \mu_2^T \lambda_2 \mu_2 - \mu_3^T \lambda_3 \mu_3 \\ & + \frac{1}{\vartheta} \sum_{i=1}^2 \left( \frac{\partial \Omega}{\partial u_i} F_i - 1 \right) \dot{\rho}_i. \end{aligned} \tag{41}$$

Using (39), we have:

$$\dot{V} \leq cV + \frac{1}{\vartheta} \sum_{i=1}^2 \left( \frac{\partial \Omega}{\partial u_i} F_i - 1 \right) \dot{\rho}_i. \tag{42}$$

In (42),  $c = \min\{2\underline{\lambda}_1, 2\underline{\lambda}_2, 2\underline{\lambda}_3\}$ , and also  $\underline{\lambda}_1$ ,  $\underline{\lambda}_2$  and  $\underline{\lambda}_3$  are the minimum eigenvalues of  $\lambda_1$ ,  $\lambda_2$  and  $\lambda_3$ , respectively. Integration (42) yields:

$$0 \leq V(t) \leq \Theta(t), \tag{43}$$

where

$$\Theta(t) = V(0)e^{-ct} + \frac{e^{-ct}}{\vartheta} \int_0^t \sum_{i=1}^2 \left( \frac{\partial \Omega}{\partial u_i} F_i - 1 \right) \dot{\rho}_i e^{c\tau} d\tau. \tag{44}$$

Considering (43) and using Lemma 1, it is obviously clear that  $\rho_i$ ,  $\int_0^t \sum_{i=1}^2 \left( \frac{\partial \Omega}{\partial u_i} F_i - 1 \right) \dot{\rho}_i e^{c\tau} d\tau$ ,  $\Theta(t)$  and  $V(t)$  are bounded. Hence, all the error signals of the overall system will be bounded. □

### 6 Simulation Results

The effectiveness of the proposed method is evaluated through a simulation study on a 3-Dof helicopter with parameters presented in Table 1. In this study, we consider 10% uncertainties on the matrices of the model to investigate the robustness of the proposed approach under uncertain conditions. As the control aim in this study is to track the desired trajectories with suitable tracking performance, we consider two distinct simulation scenarios with different reference trajectories.

**Scenario 1.** In this study, an exponential desired trajectory is considered, as follows:

$$\begin{cases} x_{d1} = 0.3 + 1.5e^{-t} - 1.8e^{-t/1.2}, \\ x_{d2} = 0.2 + e^{-t} - 1.2e^{-t/1.2}. \end{cases} \tag{45}$$

Moreover, the control parameters are selected as in Table 2. The performance of the control scheme in this scenario can be seen in Fig. 2, representing the angular motion tracking. As it is obvious from the figure, the actual signals are completely

**Table 1** Parameters of the helicopter model Lan et al. (2017b)

Parameter	Value
$k_f$	0.5 N/V
$g$	9.8m/s <sup>2</sup>
$L_a$	0.66m
$L_h$	0.177m
$J_\alpha$	0.91kg m <sup>2</sup>
$J_\gamma$	0.0364kg m <sup>2</sup>
$M_h$	1.01 kg

**Table 2** Parameters of the proposed controller

Parameter	Value
$\lambda_1$	13I <sub>2×2</sub>
$\lambda_2$	13I <sub>2×2</sub>
$\lambda_3$	13I <sub>2×2</sub>
$u_m$	3
$q$	200

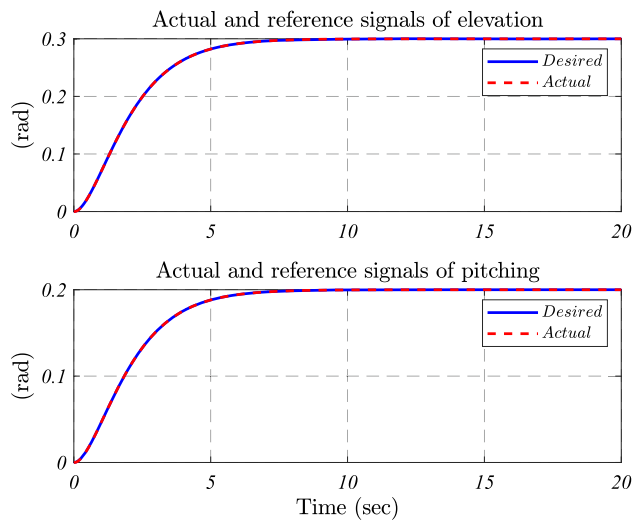


**Fig. 2** Desired and actual values of the angular positions for the first simulation scenario

converged to the desired trajectories. However, to provide further details about the quality of the tracking performance, the tracking errors are illustrated in Fig. 3. As it is demonstrated, the maximum values in the elevation and pitching channels are in the order of 10<sup>-4</sup>.

In addition, the control efforts of the front and back motors are depicted in Fig. 4. In this figure, we can see the influence of the actuator saturation in the control law where the control signals are limited to 3V, the prescribed upper limit for the control input. The signals  $u_{sat}$  in this figure are fed to the motors directly. However, in the control scheme, we have an ideal control signal  $u$ , which is a dynamic signal and it has to pass through the saturation function to produce the saturated control law  $u_{sat}$ . Figure 5 represents this control law  $u$ . As it

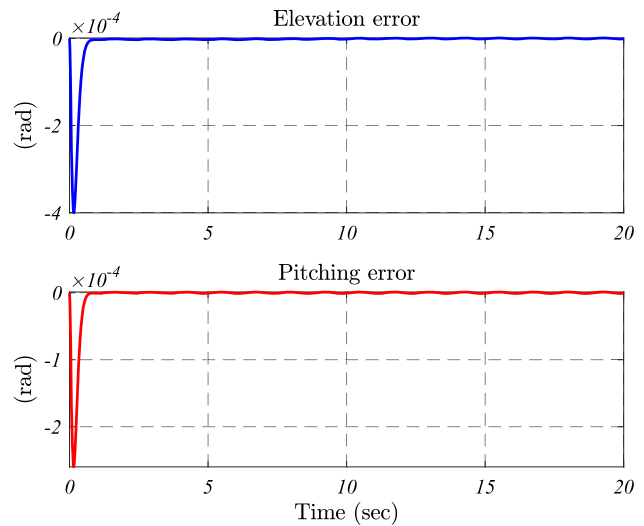


**Fig. 3** Tracking errors of the proposed scheme for the first simulation scenario

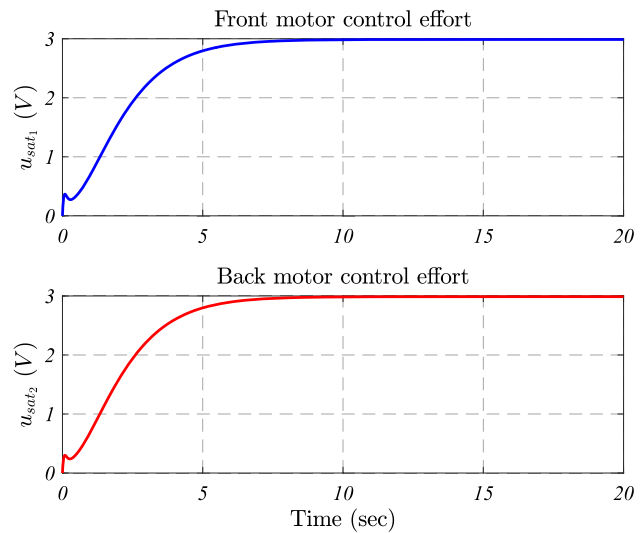


**Fig. 4** Saturated control efforts  $u_{sat}$  of the front and back motors for the first simulation scenario

is obvious, the ideal control signals have large values compared to the upper bound of the saturation function, which is affecting the actuators control efforts. Although the control law is saturated as depicted in Fig. 4, the closed-loop system can retain its suitable performance as can be seen in Fig. 3. Furthermore, the estimation errors of the adaptive RBF NN are presented in Fig. 6. Because of this suitable performance of the NN estimation, one can result in the control scheme successfully suppressing the undesirable effects of the external disturbances and the model uncertainties.

Apart from the above, the external disturbance effect can be investigated by repeating the above maneuver, while the external disturbance is added to the system in  $10 < t < 15$  as  $\zeta_\alpha = 0.01 * \sin(10t)$  and  $\zeta_\gamma = 0.01 * \sin(5t)$ . Imposing

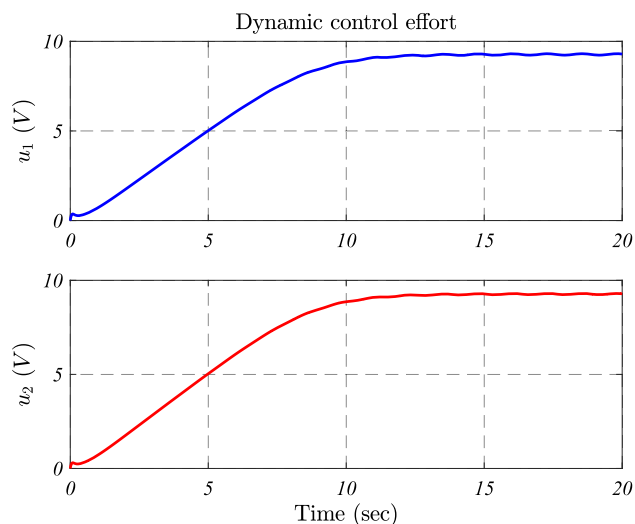


**Fig. 5** Ideal control efforts  $u$  of the front and back motors for the first simulation scenario

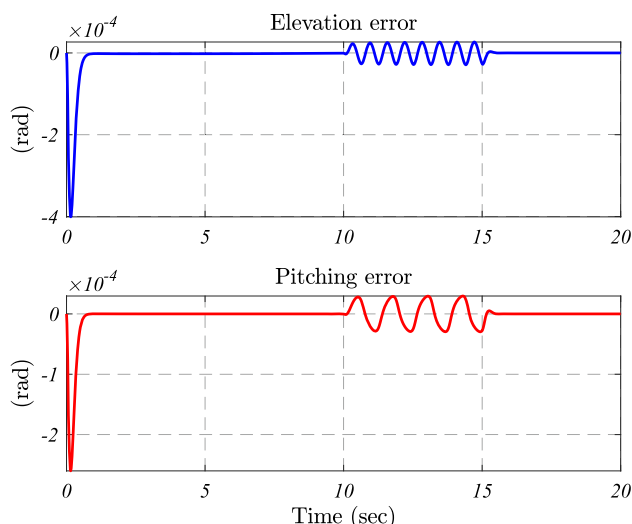


**Fig. 7** Tracking errors of the proposed scheme for the exponential scenario in the presence of external disturbance

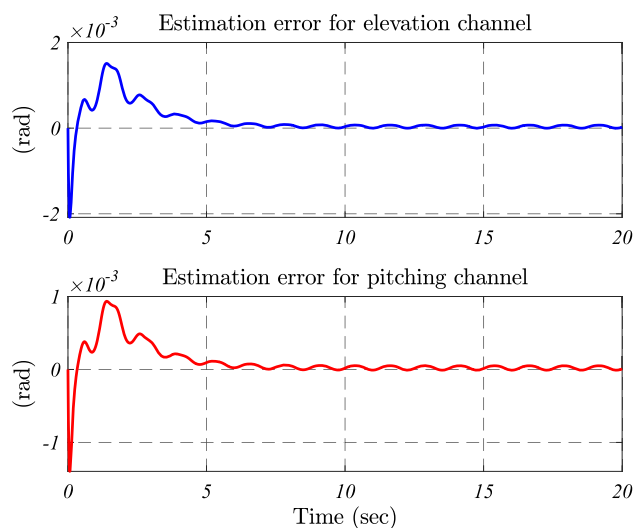


**Fig. 6** Estimation errors of the adaptive RBF NN for the first simulation scenario

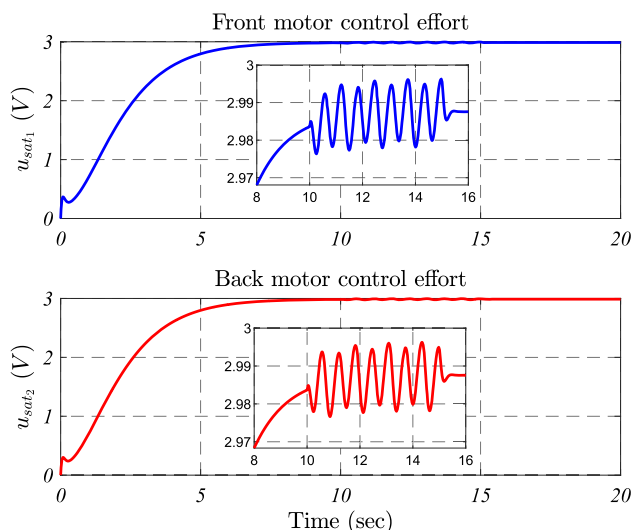


**Fig. 8** Saturated control efforts  $u_{sat}$  of the front and back motors for the exponential scenario in the presence of external disturbance

the external disturbance, the tracking errors are illustrated in Fig. 7. It can be seen that the effect of the external disturbance is successfully suppressed where the tracking errors in  $10 < t < 15$  are in the order of  $10^{-4}$  (Fig. 8).

Besides, the unsaturated ideal control signals  $u$  are illustrated in Fig. 9. In addition, the control signals for the front and back motors are demonstrated in Fig. 8. It is to be noted that these signals are passed from the prevention function that is discussed earlier. Nonetheless, achieving a suitable tracking performance according to the tracking errors in Fig. 7 shows the suitable performance of the proposed control method in the presence of the model uncertainty and external disturbance.

**Scenario 2.** In this scenario, a sinusoidal trajectory is considered to be tracked by the angular positions of the 3-DoF helicopter. Due to the periodic nature of the sinusoidal signals, such a reference path illustrates the repeatability performance of the closed-loop system. However, the initial value of the actual angular position of the helicopter is selected with a distance 0.1 rad far away from the desired trajectory, revealing the potential abilities of the method to make the system rapidly converge to the reference trajectory despite the initial difference. Furthermore, to perform this simulation study, the control parameters are the same as in the first scenario in Table 2.

By implementing this scenario, the compliance of the actual and desired signals of the helicopter angles is shown



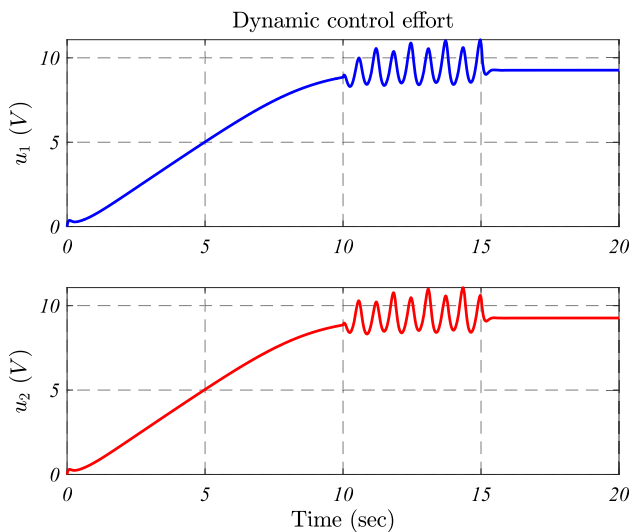


**Fig. 9** Ideal control efforts  $u$  of the front and back motors for the exponential scenario in the presence of external disturbance

**Table 3** Root-mean-square values of the tracking errors

Parameter	Value
$e_1$	$9.00 \times 10^{-3}$
$e_2$	$9.30 \times 10^{-3}$
$e_1$ (from sec 2)	$2.40 \times 10^{-6}$
$e_2$ (from sec 2)	$2.46 \times 10^{-6}$

in Fig. 10. In this figure, it is obvious that the actual signal suitably tracks the desired one. To have a better analysis of the precision of the motion tracking, the tracking errors are depicted in Fig. 11. In this figure, one can see that the initial value of the errors is equal to the distance between the desired path and the initial value of the helicopter, but before long, the steady-state errors are rapidly going to be in the order of  $10^{-6}$ , showing the fast convergence performance. The root-mean-square (RMS) values of the tracking errors are represented in Table 3. In this table, two studies are reported. In the first study, the signals are considered at all the time, but in the second study they are just considered from second 2 to the end of the time. In the RMS values of the first study, there are bigger values than the values of the second study. However, the second study just contains information on the errors in the steady state. This difference is mainly because of the initial values, which are considered on the angular positions of the helicopter.

Moreover, the saturated control law is depicted in Fig. 12. In this figure, the saturation influence has illustrated in the control input. However, as the control law is designed to be robust under the actuator saturation, we can see the suitable tracking performance in Figs. 10 and 11.

As the control law is designed based on an adaptive NN to be robust in the presence of the model uncertainties and

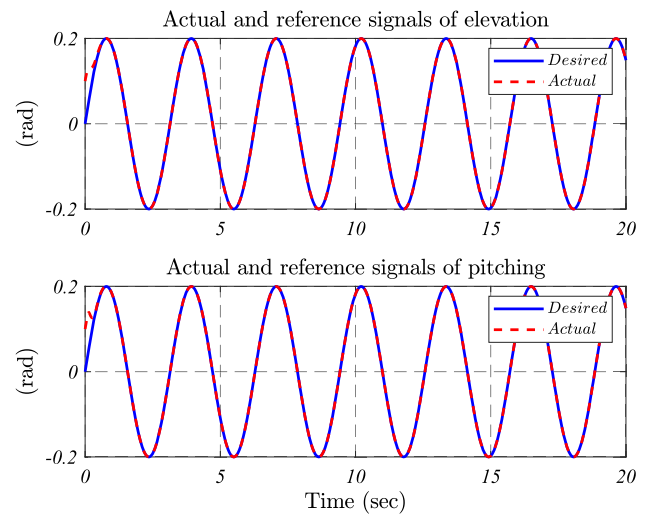


**Fig. 10** Desired and actual values of the angular positions for the sinusoidal trajectory

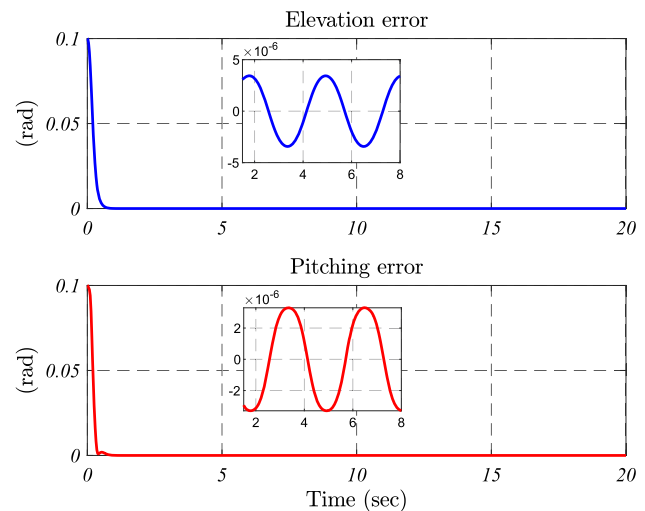


**Fig. 11** Tracking errors of the proposed scheme for the sinusoidal trajectory

external disturbances, the estimation errors are represented in Fig. 13. In this figure, the order of the estimation error is  $10^{-3}$ , which shows a suitable performance for the adaptive RBF NN.

On top of the above, this maneuver is repeated for the same setting with different initializations as the initial elevation and pitching angular positions are considered as 0.15 and 0.05, respectively. Moreover, the external disturbance is added to the system in  $10 < t < 15$  as  $\zeta_\alpha = 0.01 * \sin(10t)$  and  $\zeta_\alpha = 0.01 * \sin(5t)$ . Considering these settings, the tracking errors are demonstrated in Fig. 14. It is clear from the figure that the proposed method successfully managed to handle the initial difference between the reference signal and the initial angular position. Moreover, the effect of the external disturbance is suitably suppressed which shows the robustness

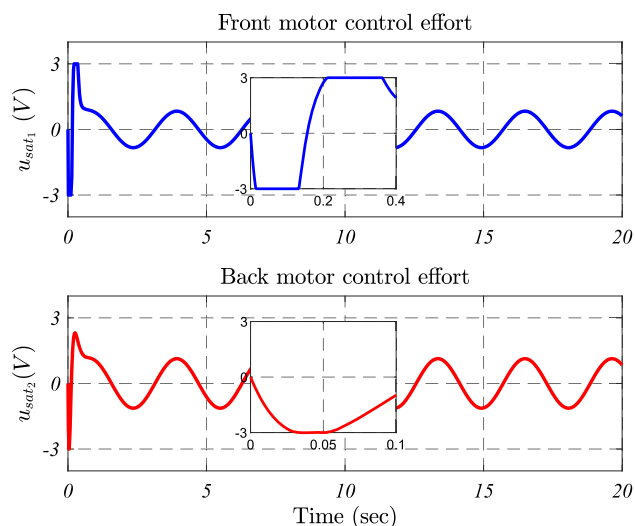


**Fig. 12** Saturated control efforts  $u_{sat}$  of the front and back motors for the sinusoidal trajectory

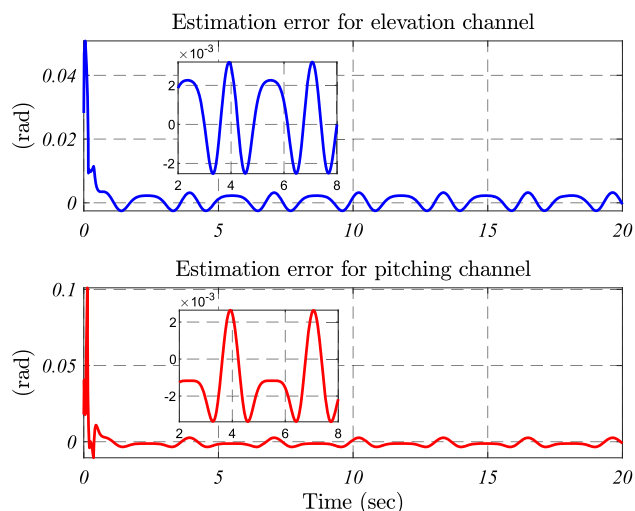


**Fig. 13** Estimation errors of the adaptive RBF NN

of the proposed method. Additionally, the saturated control efforts for the motors are exhibited in Fig. 15. In this figure, the effect of the saturation can be seen in some points, while the method represents suitable tracking performance.

### 7 Conclusion

In this paper, the dynamic surface robust control of a 3-DoF helicopter was studied in the presence of the model uncertainties, external disturbances and actuators saturation. In this study, we included the actuator saturation into the dynamic model of the system which resulted in a second-order non-affine system. To deal with the non-affine model, the control input was included in the state variables and then the third-order system was considered for the control.

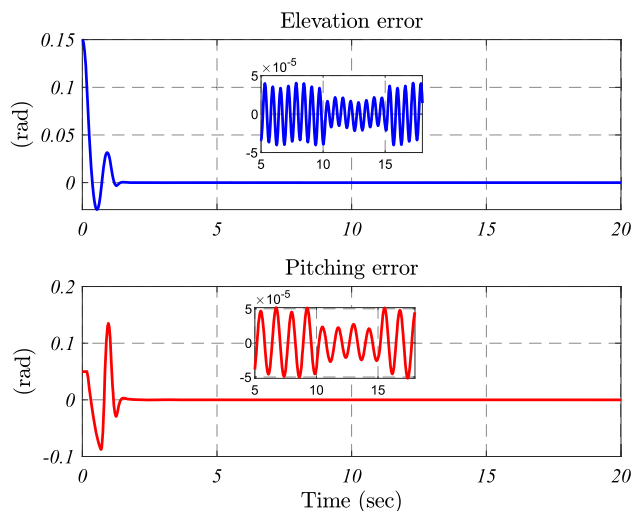


**Fig. 14** Tracking errors of the proposed scheme for the second scenario in the presence of external disturbance and different initial angular positions

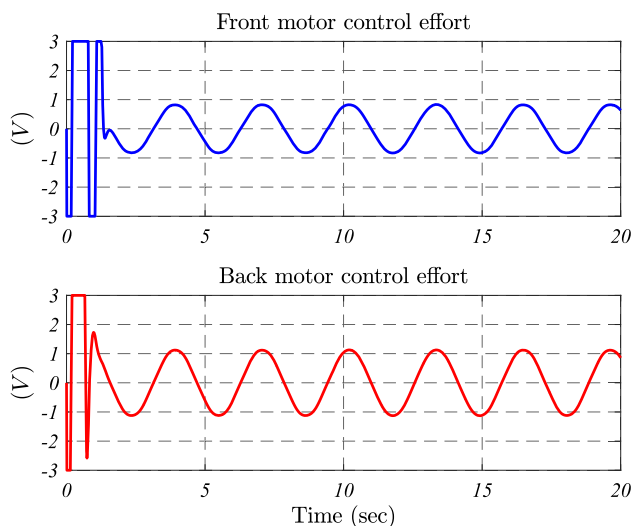


**Fig. 15** Saturated control efforts  $u_{sat}$  of the motors for the second scenario in the presence of external disturbance and different initial angular positions

For the control purpose, a backstepping control scheme was developed which was equipped with an adaptive RBF NN to be robust under undesirable effects of the uncertainties and disturbances. Furthermore, an adaptation law was proposed to adjust the NN weights. Moreover, the stability of the proposed methodology was ensured through the Lyapunov method. The results of the simulation showed suitable performance of the proposed method to deal with the actuator saturation, as well as the model uncertainties.

### Declarations

**Conflict of interest** The authors certify that there is no actual or potential conflict of interest in relation to this article.

## References

- Ameri, A., Molaei, A., & Khosravi, M.A. (2021a). Nonlinear observer-based tension distribution for cable-driven parallel robots. In *International conference on cable-driven parallel robots* (pp 105–116). Springer
- Ameri, A., Molaei, A., Khosravi, M.A., Aghdamp, Amir G. & Dargahi, Javad (2021b). Modeling and control of cable-driven parallel robots with non-affine dynamics. In *2021 60th IEEE conference on decision and control (CDC)* (pp 5582–5587). IEEE
- Ameri, A., Molaei, A., Khosravi, M. A., & Hassani, M. (2021c). Control-based tension distribution scheme for fully constrained cable-driven robots. *IEEE Transactions on Industrial Electronics*, 69(11), 11383–11393.
- Ameri, A., Fazeli, S. M., Molaei, A., Khosravi, M. A., & Hassani, M. (2023). Non-iterative positive constrained control of cable-driven parallel robots. *IEEE Transactions on Industrial Informatics*. <https://doi.org/10.1109/TII.2023.3285038>
- Bravo, R. Z. B., Leiras, A., & Cyrino Oliveira, F. L. (2019). The use of UAVs in humanitarian relief: An application of POMDP-based methodology for finding victims. *Production and Operations Management*, 28(2), 421–440.
- Bu, X. W., Wu, X. Y., Chen, Y. X., & Bai, R.-Y. (2015). Design of a class of new nonlinear disturbance observers based on tracking differentiators for uncertain dynamic systems. *International Journal of Control, Automation and Systems*, 13(3), 595–602.
- Castañeda, H., Plestan, F., Chriette, A., & de León-Morales, J. (2016). Continuous differentiator based on adaptive second-order sliding-mode control for a 3-DOF helicopter. *IEEE Transactions on Industrial Electronics*, 63(9), 5786–5793.
- Chaoui, H., & Yadav, S. (2020). Adaptive control of a 3-DOF helicopter under structured and unstructured uncertainties. *Journal of Control, Automation and Electrical Systems*, 31(1), 94–107.
- Chen, M., Shi, P., & Lim, C. C. (2015). Robust constrained control for MIMO nonlinear systems based on disturbance observer. *IEEE Transactions on Automatic Control*, 60(12), 3281–3286.
- Fazeli, S. M., Abedi, M., Molaei, A., Hassani, M., Khosravi, M. A., & Ameri, A. (2022). Active fault-tolerant control of cable-driven parallel robots. *Nonlinear Dynamics*. <https://doi.org/10.1007/s11071-022-08184-x>
- Finn, R. L., & Wright, D. (2012). Unmanned aircraft systems: Surveillance, ethics and privacy in civil applications. *Computer Law & Security Review*, 28(2), 184–194.
- Fischer, N., Kan, Z., Kamalapurkar, R., & Dixon, W. E. (2013). Saturated rise feedback control for a class of second-order nonlinear systems. *IEEE Transactions on Automatic Control*, 59(4), 1094–1099.
- Guzey, U. M., Copur, E. H., Ozcan, S., Arican, A Cagri, Kocagil, B Mahmut, & Salamci, Metin U. (2019). Experiment of sliding mode control with nonlinear sliding surface design for a 3-DOF helicopter model. In *2019 XXVII international conference on information, communication and automation technologies (ICAT)* (pp. 1–6). IEEE
- Jawhar, I. H., Mohamed, N., Trabelsi, Z., & Al-Jaroodi, J. (2016). Architectures and strategies for efficient communication in wireless sensor networks using unmanned aerial vehicles. *Unmanned Systems*, 4(04), 289–305.
- Kanistras, K., Martins, G., Rutherford, M.J., Valavanis, Kimon P. (2013). A survey of unmanned aerial vehicles (UAVs) for traffic monitoring. In *2013 international conference on unmanned aircraft systems (ICUAS)* (pp 221–234). IEEE
- Lan, J., Patton, R. J., & Punta, E. (2017). Fault-tolerant tracking control for a 3-DOF helicopter with actuator faults and saturation. *IFAC-PapersOnLine*, 50(1), 5250–5255.
- Lan, J., Patton, R. J., & Zhu, X. (2017). Integrated fault-tolerant control for a 3-DOF helicopter with actuator faults and saturation. *IET Control Theory & Applications*, 11(14), 2232–2241.
- Li, C., Yang, X., Sun, Y. & Lin, Weiyang. (2018). Robust output feedback control for a 3-DOF helicopter system. In *IECON 2018-44th annual conference of the IEEE industrial electronics society* (pp 5513–5518). IEEE
- Li, Z., Liu, H. H., Zhu, B., & Gao, H. (2015). Robust second-order consensus tracking of multiple 3-DOF laboratory helicopters via output feedback. *IEEE/ASME Transactions on Mechatronics*, 20(5), 2538–2549.
- Lin, W. (1995). Input saturation and global stabilization of nonlinear systems via state and output feedback. *IEEE Transactions on Automatic Control*, 40(4), 776–782.
- Liu, Y. H. (2017). Saturated robust adaptive control for uncertain non-linear systems using a new approximate model. *IET Control Theory & Applications*, 11(6), 870–876.
- Meza-Sánchez, M., Aguilar, L. T., & Orlov, Y. (2015). Output sliding mode-based stabilization of underactuated 3-DOF helicopter prototype and its experimental verification. *Journal of the Franklin Institute*, 352(4), 1580–1594.
- Mousavi, S. H., & Khayatian, A. (2011). Dead zone model based adaptive backstepping control for a class of uncertain saturated systems. *IFAC Proceedings Volumes*, 44(1), 14489–14494.
- Mousavi, S. H., & Khayatian, A. (2016). Dead-zone model based adaptive backstepping control for a class of uncertain saturated systems. *Asian Journal of Control*, 18(4), 1395–1405.
- Park, J., & Sandberg, I. W. (1991). Universal approximation using radial-basis-function networks. *Neural Computation*, 3(2), 246–257.
- Ponce, I.U., Flores-Abad, A., & Nandayapa, M. (2018). Robust control of a 3-DOF helicopter with input dead-zone. In *Advanced topics on computer vision, control and robotics in mechatronics* (pp 265–287). Springer
- Saska, M., Krátký, V., Spurný, V., Báča, T. (2017). Documentation of dark areas of large historical buildings by a formation of unmanned aerial vehicles using model predictive control. In *2017 22nd IEEE international conference on emerging technologies and factory automation (ETFA)* (pp 1–8). IEEE
- Wen, C., Zhou, J., Liu, Z., & Su, H. (2011). Robust adaptive control of uncertain nonlinear systems in the presence of input saturation and external disturbance. *IEEE Transactions on Automatic Control*, 56(7), 1672–1678.
- Zheng, Z., Huang, Y., Xie, L., & Zhu, B. (2017). Adaptive trajectory tracking control of a fully actuated surface vessel with asymmetrically constrained input and output. *IEEE Transactions on Control Systems Technology*, 26(5), 1851–1859.
- Zhu, B., Zhang, Q., & Liu, HHT. (2015). A comparative study of robust attitude synchronization controllers for multiple 3-DOF helicopters. In: *2015 American Control Conference (ACC)* (pp 5960–5965). IEEE
- Zhu, X., & Li, D. (2021). Robust attitude control of a 3-DOF helicopter considering actuator saturation. *Mechanical Systems and Signal Processing*, 149, 107209.

**Publisher's Note** Springer Nature remains neutral with regard to jurisdictional claims in published maps and institutional affiliations.

Springer Nature or its licensor (e.g. a society or other partner) holds exclusive rights to this article under a publishing agreement with the author(s) or other rightsholder(s); author self-archiving of the accepted manuscript version of this article is solely governed by the terms of such publishing agreement and applicable law.